Detection, Localization, and Conformational Analysis of Single Polysaccharide Molecules on Live Bacteria

Grégory Francius,[†,¶] Sarah Lebeer,[‡,¶] David Alsteens,[†] Linda Wildling,[§] Hermann J. Gruber,[§] Pascal Hols,[⊥] Sigrid De Keersmaecker,[‡] Jos Vanderleyden,[‡] and Yves F. Dufrêne[†,*]

[†]Unité de Chimie des Interfaces, Université Catholique de Louvain, Croix du Sud 2/18, B-1348 Louvain-la-Neuve, Belgium, [‡]Centre of Microbial and Plant Genetics and INPAC, K.U.Leuven, Kasteelpark Arenberg 20, 3001 Leuven, Belgium, [§]Institute of Biophysics, Johannes Kepler University of Linz, Altenbergerstr.69, A-4040 Linz, Austria, and [⊥]Unité de Génétique, Institut des Sciences de la Vie, Université catholique de Louvain, Croix du Sud 5/6, B-1348 Louvain-la-Neuve, Belgium. [¶]These authors contributed equally to this work.

ABSTRACT The nanoscale exploration of microbes using atomic force microscopy (AFM) is an exciting, rapidly evolving research field. Here, we show that single-molecule force spectroscopy is a valuable tool for the localization and conformational analysis of individual polysaccharides on live bacteria. We focus on the clinically important probiotic bacterium *Lactobacillus rhamnosus* GG, demonstrating the power of AFM to reveal the coexistence of polysaccharide chains of different nature on the cell surface. Applicable to a wide variety of cells, this single molecule method offers exciting prospects for analyzing the heterogeneity and diversity of macromolecules constituting cell membranes and cell walls.

KEYWORDS: atomic force microscopy · elasticity · bacteria · lectins · mutants · polysaccharides · single-molecule force spectroscopy

Polysaccharides on bacterial surfaces fulfill several important functions, such as protecting the cell against unfavorable environmental conditions, mediating cellular recognition (*e.g.*, *via* lectin binding), and promoting bacterial adhesion and biofilm formation on inert or living surfaces.[1−5] Although elucidation of the complexity and diversity of the chemical structures of cell wall associated polysaccharides is progressing, studying their spatial organization and conformational properties at the molecular level remains a challenge.

For centuries, lactic acid bacteria from the genus *Lactobacillus* have played an important role in fermentations. Currently, increasing attention is given to their probiotic, health-promoting effects, as they are also members of the beneficial microbiota present in the human gastrointestinal and urogenital tract.[6] Among these probiotic bacteria, *Lactobacillus rhamnosus* strain GG (LGG)[7] is one of the best clinically investigated organisms. It is postulated that some of its health effects[7] are related to its strong adhesive capacity to epithelial cells[8] and mucus.[9] Recently, it was shown that LGG is able to form biofilms on abiotic surfaces, in contrast to other strains of the *Lactobacillus casei* group tested under the same conditions.[10] Different factors were reported to contribute to biofilm formation, including production of exopolysaccharides.[10,11] Despite the increasing number of clinical studies demonstrating that probiotics such as LGG can improve health, little is known about causal relationships between health effects and cell surface interactions. This emphasizes the need to develop methods to quantify the molecular characteristics of the cell surface of these probiotic strains.

The nanoscale exploration of microbial cells using atomic force microscopy (AFM) is an exciting research field that has developed tremendously in the past years.[12,13] While real-time AFM imaging enables investigators to visualize the ultrastructure of hydrated cells,[14−18] AFM force spectroscopy offers a means to probe a variety of properties, such as cell wall elasticity,[19−22] the distribution and interaction forces of chemical groups,[23,24] and the localization of single molecular recognition sites.[25−28] Importantly, recent progress in single molecule force spectroscopy (SMFS) has allowed researchers to probe the conformational properties of microbial polysaccharides.[29−31] Here, we demonstrate the ability of SMFS to detect, map, and analyze individual polysaccharide

*Address correspondence to Yves.Dufrene@uclouvain.be.

Received for review June 4, 2008 and accepted August 04, 2008.

Published online August 16, 2008.
10.1021/nn800341b CCC: $40.75

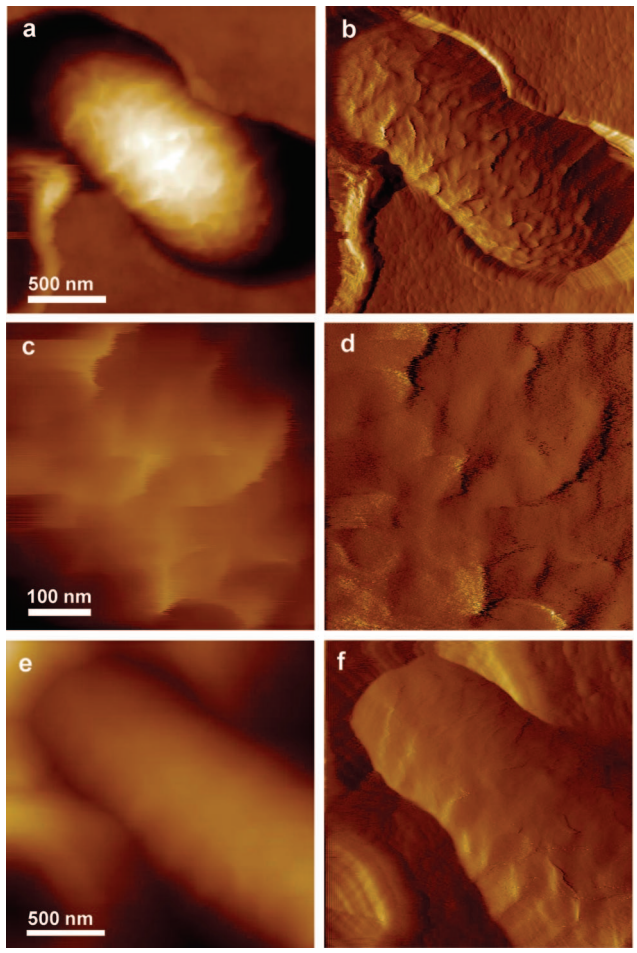

Figure 1. Imaging single LGG bacteria in their native state. AFM height (a,c,e) and deflection (b,d,f) images recorded in buffered solution (PBS) for LGG wild-type (a−d) and for the mutant CMPG5413 impaired in cell wall polysaccharide production (e,f). Cells were trapped into a porous polymer membrane for noninvasive, *in situ* imaging.

molecules on live LGG bacteria. We show that the polysaccharide properties (distribution, adhesion, extension) of LGG wild-type are markedly different from those of a derived mutant (strain CMPG5413) impaired in adherence to gut epithelium, biofilm formation, and exopolysaccharide production.[11,32]

RESULTS AND DISCUSSION

To gain insight into the LGG surface morphology, live bacterial cells were immobilized in porous membranes[33,34] and imaged in their native state using AFM (Figure 1). While the resolution of height images was limited by the large curvature of these rod-shaped cells, deflection images were more sensitive to the surface relief. For LGG wild-type (Figure 1a−d), AFM images revealed a rough morphology decorated with waves 15 ± 7 nm high and separated by 123 ± 59 nm (n = 40). This differs from the morphology reported for the round-shaped lactic acid bacterium *Lactococcus lactis*, where tip-cell interactions were shown to dominate the image contrast.[35] The scanning tip was shown to alter the *L. lactis* surface by forming grooves and sponge-like structures. None of these effects were observed here and the wave-like morphology on the LGG wild-type could be imaged repeatedly without being altered, indicating the observed contrast reflects real surface features. By contrast, the mutant (Figure 1e,f) showed a much smoother morphology (rms roughness on 500 nm × 500 nm areas of 1.2 ± 0.3 nm, compared to 3.6 ± 0.7 nm for the wild-type), with much less pronounced waves that were 5 ± 2 nm high and separated by 80 ± 37 nm. In line with previous phenotypic analyses of this mutant showing abolished exopolysaccharide production and biofilm formation,[11,32] it seems likely that the surface wave-like structures observed on LGG wild-type reflect the production of extracellular polysaccharides, which is greatly reduced in the mutant CMPG5413. This interpretation is consistent with earlier AFM analyses of *Lactobacillus* strains[14] which revealed that cells covered with a regular lattice of globular proteins, like an S-layer, are smooth on a length scale of a few nm, while polysaccharide-coated cells show heterogeneous and rough surfaces. The observed wave-like structures in LGG might reflect the helical-mode of cell wall synthesis reported for rod-shaped bacteria,[36,37] in contrast to coccoid cells, such as *L. lactis*, where new cell wall material is inserted at the division septum.

To explore the cell wall nanomechanical properties, force−distance curves were recorded, converted into force−indentation curves, and then analyzed using the Hertz theory to generate elasticity maps and histograms.[38,39] Figure 2 shows low and high resolution elasticity maps of the two strains, together with elasticity histograms and typical force-indentation curves recorded on top of the cells. Most curves were well-described by the Hertz model, allowing us to obtain Young modulus values. Unlike Gaboriaud *et al.*,[21] we did not observe two regimes, that is, a nonlinear domain at low loading forces, followed by a linear one at high loading forces. This may be because we kept the maximum loading force at rather low values (1 nN) to avoid detachment of the cells from the membrane. The elasticity contrast demonstrates that the cells were substantially softer than the supporting polymer membrane (brighter contrast, Young modulus ≈ 1 MPa). The curves recorded across the cells yielded Young modulus of 186 ± 40 kPa and 300 ± 63 kPa for the wild-type and mutant, respectively. Elasticity maps recorded on cells showed homogeneous contrast, indicating that curvature/edge effects did not substantially influence the shape of the curves and the obtained elasticity values. Hence, our data show that extracellular polysaccharides play a crucial role in determining the surface elasticity and softness of the cell surface of wild-type LGG. The mutant appears two times stiffer compared to the wild-type. This suggests that the nanomechanical properties of the mutant were essentially determined by peptidoglycan, which is covered by ex-

opolysaccharides in the wild-type. Peptidoglycan is a stiff polymer due to the high cross-linking density and limited conformational flexibility of the β 1−4 linkage between *N*-acetylglucosamine and *N*-acetylmuramic acids.

Next, we probed individual cell surface polysaccharides using SMFS with lectin-modified tips to address the following pertinent question: what is the heterogeneity of the polysaccharides in terms of distribution across the cell surface and in terms of different macromolecules? To this end, AFM tips functionalized with *Pseudomonas aeruginosa* (PA-1) and concanavalin A (Con A) lectins were used to specifically detect polysaccharide molecules containing galactose and mannose (or glucose), respectively. To validate the method, force curves were recorded between Con A-modified tips and agarose beads functionalized with mannose residues (Figure 3a). As shown in Figure 3b, a significant fraction of the curves displayed single adhesion forces at short rupture distances (0−50 nm), the remaining measurements exhibiting no adhesion. The corresponding adhesion force histogram displayed a well-defined maximum at 57 ± 19 pN that we attribute to the rupture of single lectin−mannose complexes. The specificity of the measured forces was demonstrated by showing a dramatic reduction of adhesion frequency when the curves were recorded in the presence of free mannose (Figure 3c).

We then used the Con A and PA-1-terminated tips to probe the distribution, adhesion, and extension of the surface polysaccharides of the LGG wild-type and mutant strains. Figure 4a−d show the adhesion map, adhesion histogram, and force curves obtained on the wild type with a Con A-tip. The curves showed essentially single adhesion events, along with elongation forces and rupture lengths ranging from 20 to 400 nm that were well-fitted with an extended freely jointed chain model.[40,41] The distribution of adhesion forces showed a well-defined maximum at 56 ± 20 pN, that is, close to the mannose values (Figure 3b), suggesting these forces reflected single ConA−mannose interactions. Adhesion forces in the 100−200 pN range were also frequently observed and attributed to the simultaneous detection of two or three residues. Force curves recorded in the presence of free mannose showed a dramatic reduction of adhesion frequency (from 93% to 43%), supporting the notion that specific forces were measured (data not shown). Like the elasticity distribution, the polysaccharide distribution was rather homogeneous and did not depend on the heterogeneous surface morphology. Taken together, the above observations indicate that mannose (or glucose)-rich polysaccharide molecules were detected and stretched on the LGG surface.

Notably, the CMPG5413 mutant showed a very different behavior (Figure 4e−h), in that (i) the adhesion maps and force histograms showed a dramatic reduction of adhesion frequency; (ii) consistent with this, adhesion forces greater than 100 pN were rarely

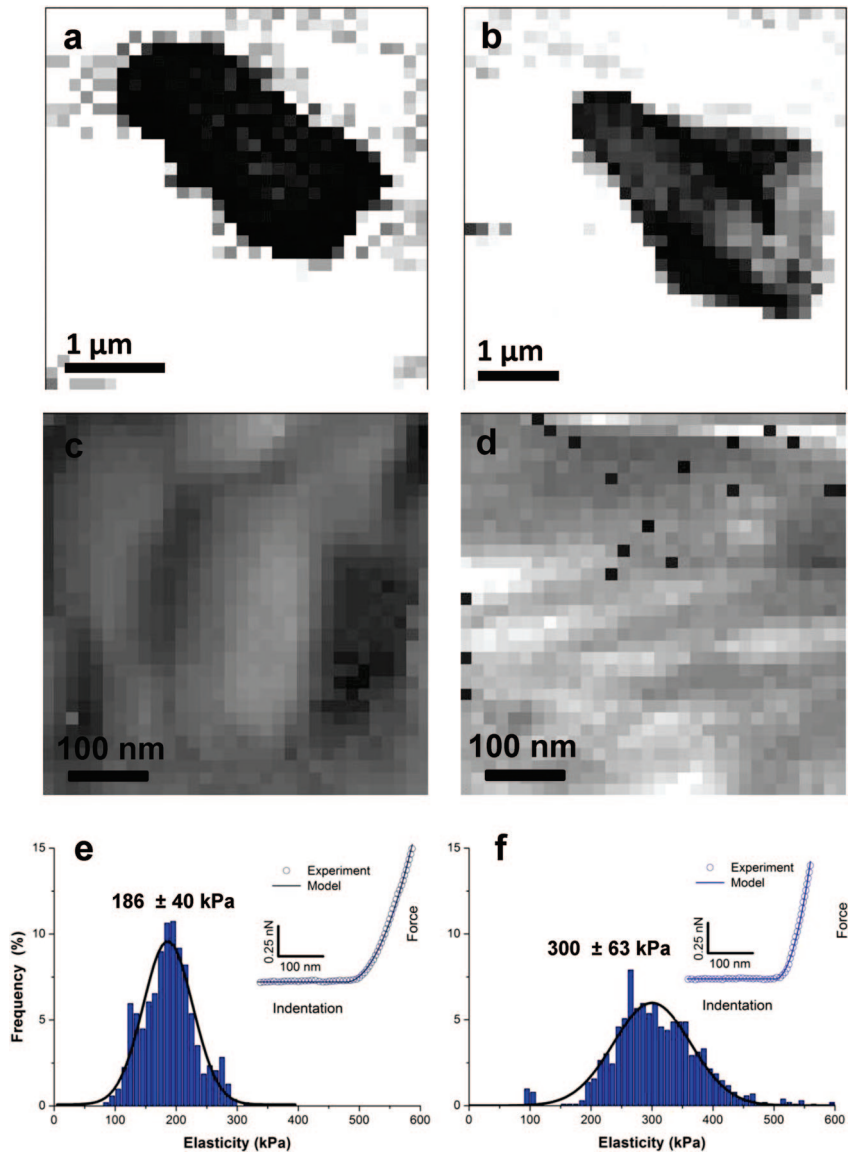

Figure 2. Mapping cell surface nanomechanical properties. (a, b) Low resolution elasticity maps (z-range = 1 MPa) recorded on LGG wild-type (a) and on the mutant (b). (c, d) High resolution elasticity maps (z-range = 0.5 MPa), together with (e, f) elasticity histograms and typical force-indentation curves recorded on top of LGG wild-type (c, e) and of the mutant (d, f) (open symbols are raw data while the solid line shows the theoretical fit using the Hertz model).

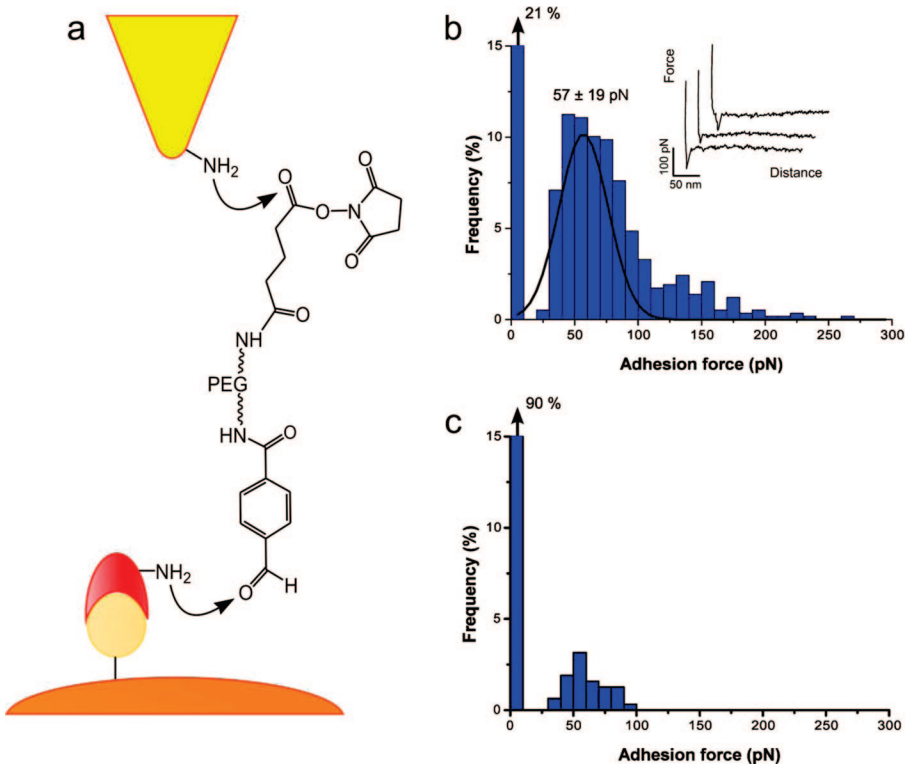

Figure 3. Use of lectin-terminated tips for detecting single carbohydrate residues. (a) Surface chemistry used to functionalize AFM tips with lectins. (b) Representative force curves and adhesion force histogram (n = 586) obtained in buffered solution (sodium acetate + 1 mM $CaCl_2$ + 1 mM $MnCl_2$) between a concanavalin A-terminated tip and a mannose-terminated agarose bead. (c) Control experiment showing a dramatic reduction of adhesion frequency when the force measurements are performed in the presence of free mannose (100 mM).

observed indicating that only single residues were detected at a time; and (iii) most rupture distances were short, typically in the 0−100 nm range. These single molecule analyses, consistent with the structural and elasticity data, demonstrate that the two strains show very different polysaccharide properties, the surface density and extension of mannose-rich polysaccharides being much higher on the wild-type than on the mutant. To better visualize differences in polysaccharide properties, three-dimensional maps were constructed by combining adhesion forces (false colors, yellow meaning larger adhesion forces) and rupture distances (z level) measured at every x, y location (Figure 4d,h).

The SMFS data obtained on the wild-type with a PA-1-tip are shown in Figure 5a−d. Similar to what we observed with the ConA-tips, adhesion forces were homogeneously distributed across the cell surface (Figure 5c) and showed a well-defined maximum at 51 ± 24 pN (Figure 5b) attributed to single PA-1-galactose interactions that could be blocked with free galactose (data not shown). Larger adhesion forces due to multiple interactions were observed as well. However, the curves obtained with the PA-1 tips showed multiple adhesion peaks (Figure 5b), with much longer rupture distances, typically in the 100−1000 nm range (Figure 5d). For the mutant (Figure 5e−h), again we found a reduction of adhesion frequency, and much shorter rupture distances (0−200 nm), demonstrating that the surface density and extension of galactose-rich polysaccharides were dramatically reduced compared with those of the wild-type.

Taken together, these data suggest that polysaccharides probed with ConA and PA-1 tips were of different nature, that is, mannose-rich polysaccharide chains showing single rupture forces with moderate extensions and galactose-rich polysaccharide chains showing multiple ruptures and much longer extensions (Figure 6). The occurrence of galactose-rich polysaccharides is fully consistent with previously published structural studies[42] and with our own biochemical analyses (unpublished data) revealing that LGG produces exopolysaccharides mainly composed of D-galactose, with small amounts of L-rhamnose and *N*-acetyl-D-glucosamine residues. The nature of the second polysaccharide detected with the ConA tip is currently unknown. In fact, to the best of our knowledge, this SMFS study is the first to show the occurrence of a second abundant polysaccharide present on the cell surface of LGG, supporting further the novelty of this study. It remains to be elucidated whether the mannose (or glucose)-rich polysaccharide on the cell surface of LGG represents a polysaccharide chain on an abundant glycoprotein or a second, shorter and more strongly associated cell wall polysaccharide different from the previously reported exopolysaccharide of LGG.[42]

CONCLUSIONS

In summary, the AFM data presented here demonstrate the crucial role played by cell wall polysaccharides in determining the nanoscale surface properties of LGG bacteria. We show that LGG wild-type and the CMPG5413 mutant impaired in adherence, biofilm formation, and polysaccharide production display very different surface morphology, surface elasticity, and polymer properties. The wave-like patterns observed on the wild-type, reflecting the massive production of cell wall polysaccharides, are

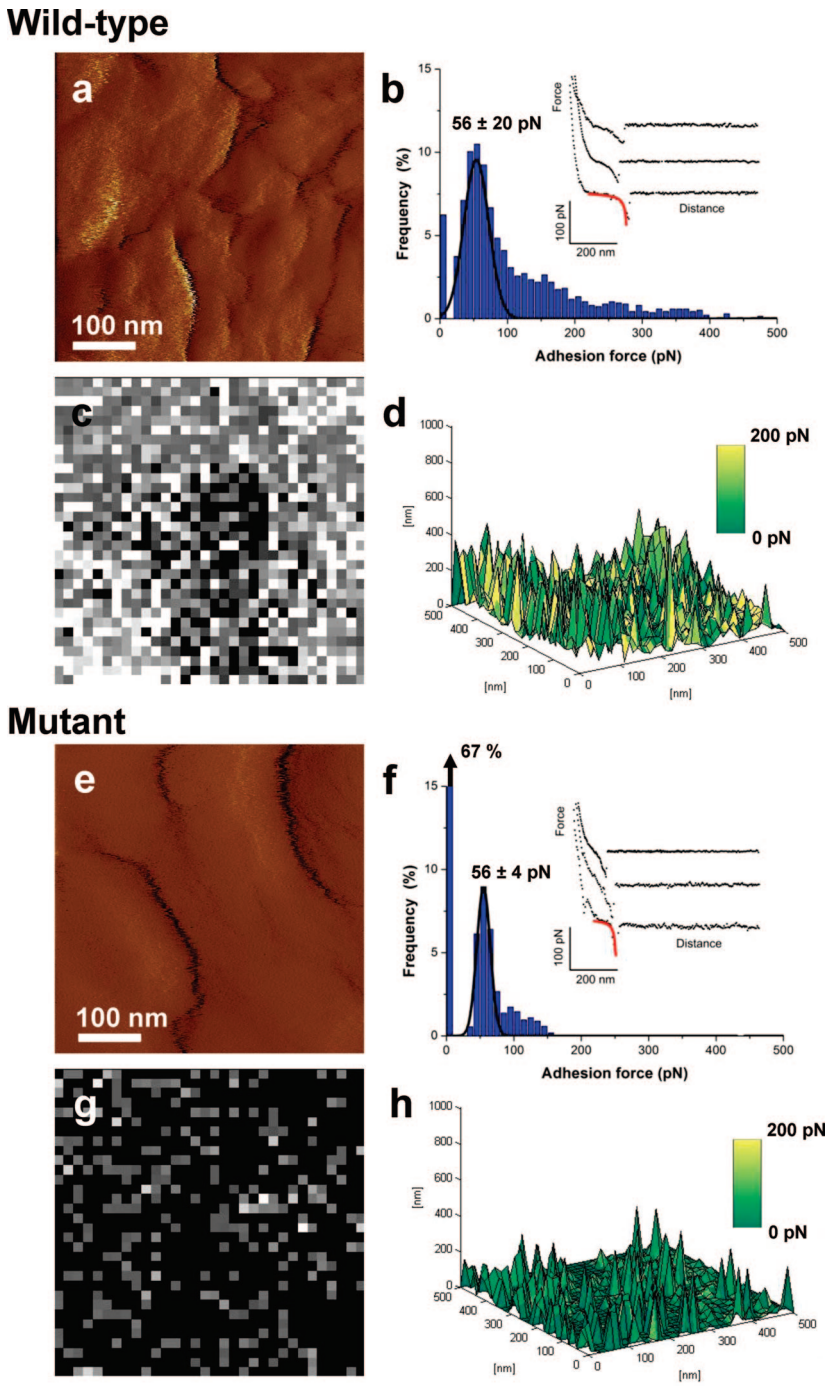

Figure 4. Detecting individual mannose (or glucose)-rich polysaccharides on LGG bacteria. (a, e) AFM deflection images, (b, f) adhesion force histograms (n = 1024) together with representative force curves, and (c, g) adhesion force maps (gray scale: 200 pN) recorded in buffered solution (sodium acetate + 1 mM $CaCl_2$ + 1 mM $MnCl_2$) with a Con A tip on LGG wild-type (a−c) and on the mutant CMPG5413 (e−g). (d, h) To compare polysaccharide properties on the two strains, three-dimensional reconstructed maps were obtained by combining adhesion force values (expressed as false colors) and rupture distances (expressed as z level) measured at different x, y locations. The red lines on the bottom curves in panels b and f show that elongation forces were well-described by an extended freely jointed chain model with Kuhn lengths of 1.2 ± 0.3 (b) and 1.4 ± 0.3 nm (f), and segment elasticities of 0.6 ± 0.5 (b) and 5.0 ± 5.5 N/m (f): $x(F) = L_c\,[\coth(Fl_k/k_bT) - k_bT/Fl_k][1 + nF/k_sL_c]$, where L_c and l_k are the contour length and Kuhn length of the molecule, n and k_s are the number of segments and their elasticity, k_b is the Boltzmann constant, and T is the absolute temperature.

much less pronounced on the mutant. Consistent with these structural data, the wild-type shows a softer cell surface and polysaccharide chains that are much longer and more densely distributed on the surface compared to the mutant. Additionally, two kinds of polysaccharide molecules are identified on LGG wild-type, that is, polysaccharides rich in mannose (possibly also in glucose) having moder-

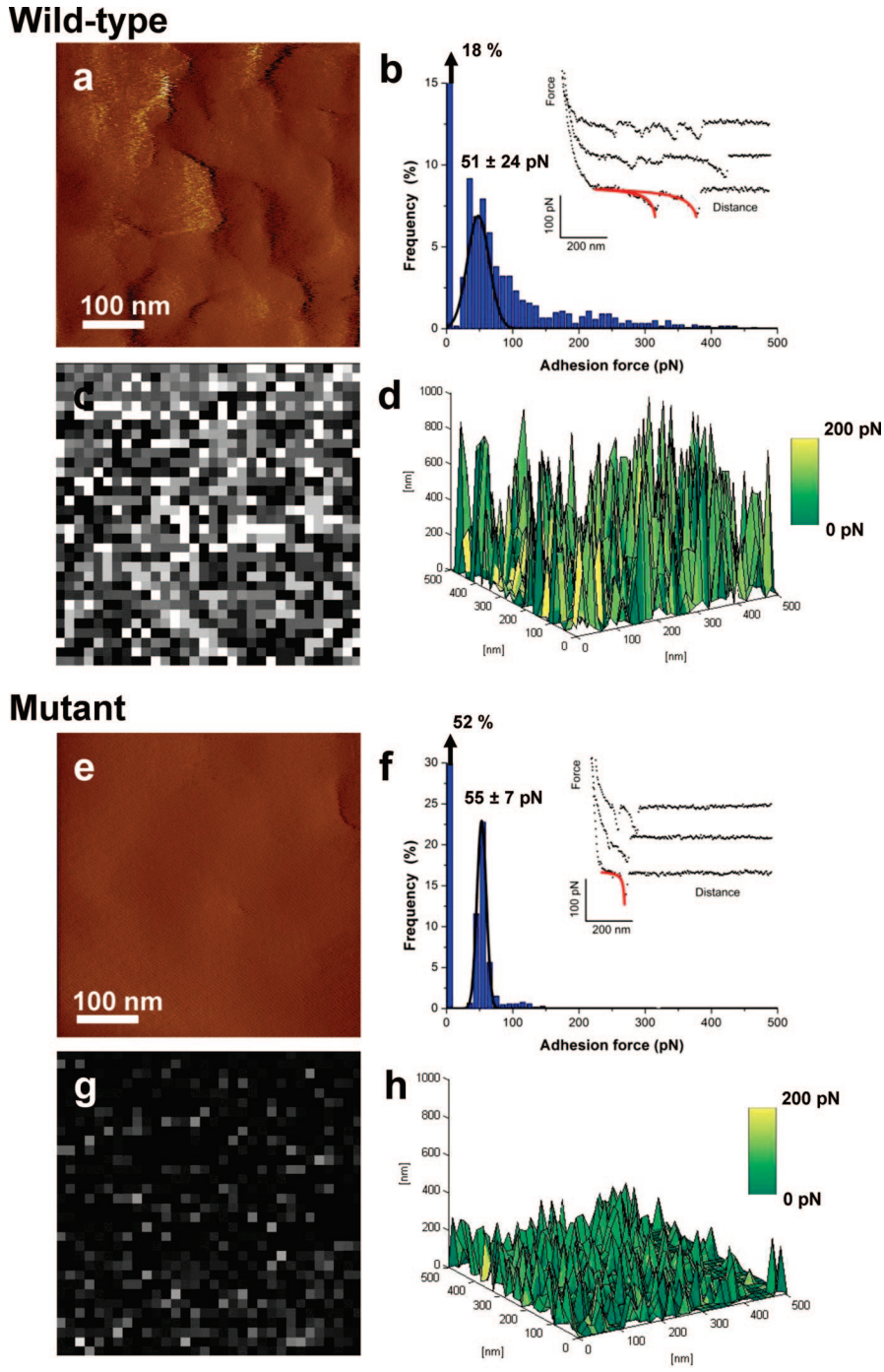

Figure 5. Detecting individual galactose-rich polysaccharides on LGG bacteria. (a, e) AFM deflection images, (b, f) adhesion force histograms (n = 1024) together with representative force curves and (c, g) adhesion force maps (gray scale: 200 pN) recorded with a PA-1 tip on LGG wild-type (a−c) and on the mutant CMPG5413 (e−g). (d, h) Three dimensional reconstructed maps obtained by combining adhesion force values and rupture distances measured at different x, y locations. The red lines on the bottom curves in panels b and f show that elongation forces were well-described by an extended freely jointed chain model with Kuhn lengths of 1.4 ± 0.2 (b) and 1.7 ± 0.3 nm (f), and segment elasticities of 1.1 ± 0.8 (b) and 1.2 ± 1.5 N/m (f).

ate extensions and polysaccharides rich in galactose having much longer extensions, which were significantly altered in the mutant (Figure 6). In the future, SMFS-based phenotypic analyses of different mutants hold great promise in understanding the resulting changes in spatial and conformational properties of cell wall-constituting macromolecules. Particularly, SMFS is a powerful tool to study the remarkable polysaccharide properties of LGG in relation to the functions of the cell surface, such as bacterial adhesion to intestinal tissues, and interactions with specific receptors of the immune system.

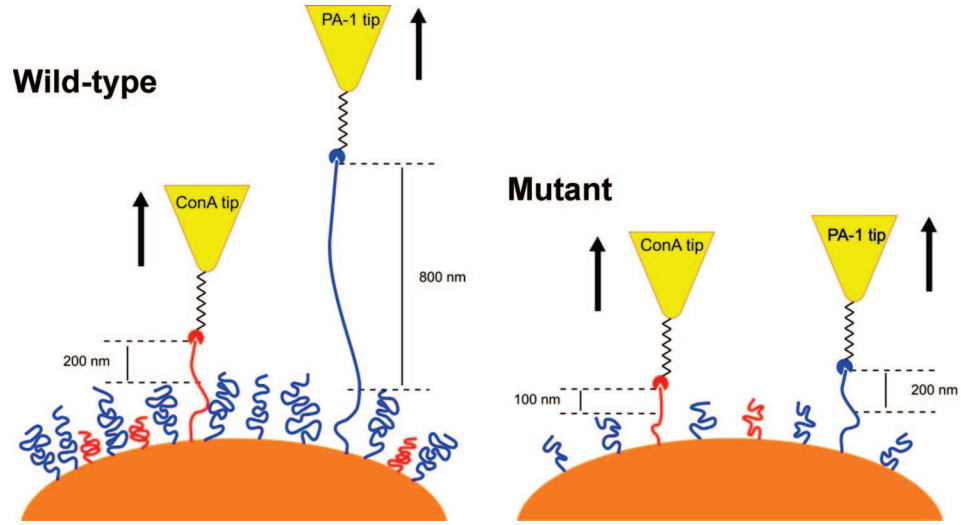

Figure 6. Spatial organization and conformational properties of the different polysaccharide molecules detected on LGG using Con A- and PA-1-terminated tips. Two kinds of polysaccharide chains were identified on LGG wild-type (left): polysaccharides rich in mannose having moderate extensions (red), and polysaccharides rich in galactose having much longer extensions (blue). Compared to the wild-type, the mutant showed polysaccharide chains that were much shorter and more loosely distributed on the surface (right).

METHODS

L. rhamnosus GG (ATCC 53103) and the CMPG5413 mutant were grown in lactobacilli AOAC medium (Difco) to enhance polysaccharide production as previously described.[10,32] Cells were centrifuged (7000 rpm for 10 min) and washed twice by resuspension in PBS and centrifugation.

AFM images and force−distance curves were recorded at room temperature (20 °C) in buffered solutions (PBS, pH = 7.4 or sodium acetate containing 1 mM $CaCl_2$ + 1 mM $MnCl_2$, pH 4.75) using a Nanoscope IV Multimode AFM (Veeco Metrology Group, Santa Barbara, CA) and oxide-sharpened microfabricated Si_3N_4 cantilevers (Microlevers, Veeco Metrology Group, Santa Barbara, CA). Cells were immobilized by mechanical trapping into porous polycarbonate membranes (Millipore), with a pore size similar to the bacterial cell size (about 1.2 μm diameter).[33,34] The spring constants of the cantilevers measured using the thermal noise method (Picoforce, Veeco Metrology Group) were found to be 0.011 N/m. Blocking experiments were performed by adding respectively 100 mM D-(+)-mannose and 100 mM D-(+)-galactose to the solutions. Experiments on model carbohydrate surfaces were performed on agarose beads functionalized with D-mannose (Sigma-Aldrich). Single molecule force spectroscopy measurements were performed using a constant approach and retraction speed of 1,000 nm/s and a maximum applied force of 500 pN.

Mechanical properties were mapped by recording force−volume images consisting of arrays of 32 × 32 force curves, using a maximum applied force of ~1 nN. Elasticity maps and histograms were generated by analyzing the force curves according to the Hertz theory for elastic media, using a conical tip geometry:

$$F = \frac{2E \tan \alpha}{\pi(1-\nu^2)}\delta^2 \qquad (1)$$

where F is the force, δ is the indentation depth, E is the Young modulus, ν is the Poisson coefficient and α is the semi-top angle of the tip. A program developed for soft materials in Fortran C++ (Compaq Visual Fortran V.6.6, Compaq Computer Corp., Houston, TX) was adapted and used to fit the experimental force curves with the model. More details on data treatment can be found elsewhere.[19,43] High-resolution elasticity maps were obtained on single bacteria by recording 500 nm × 500 nm force−volume images on top of the cell, thereby minimizing possible curvature/edge effects.

For probing cell surface polysaccharides, AFM tips were functionalized with the lectin concanavalin A (Con A; Sigma-Aldrich) and the lectin from *Pseudomonas aeruginosa* (PA-I, Sigma-Aldrich) *via* a 6 nm-long polyethylene glycol (PEG) chain. Cantilevers were washed with chloroform and ethanol, placed in an UV-ozone-cleaner for 30 min, and immersed overnight in a solution of ethanolamine hydrochloride in DMSO (3.3 g in 6 mL) to generate amino groups on the tip surface.[44] These amino groups were further reacted with PEG linkers carrying benzaldehyde functions on their free-tangling end, essentially as described in ref 45. For coupling of proteins, the cantilever was covered with a 200 μL droplet of a PBS solution containing Con A (0.2 mg/mL) to which 2 μL of a 1 M $NaCNBH_3$ solution was added.[45] After 50 min of incubation, 5 μL of a 1 M ethanolamine hydrochloride solution (preadjusted to pH 9.5 with NaOH, see Supporting Information to ref 45) was added in order to deactivate unreacted aldehyde groups during another 10 min incubation period, after which the cantilever was washed with and stored in PBS.

Acknowledgment. This work was supported by the National Foundation for Scientific Research (FNRS), the Université catholique de Louvain (Fonds Spéciaux de Recherche), the Région wallonne, the Federal Office for Scientific, Technical and Cultural Affairs (Interuniversity Poles of Attraction Programme), the Research Department of the Communauté française de Belgique (Concerted Research Action) and Fonds voor Wetenschappelijk Onderzoek-Vlaanderen (FWO). Y.F.D. and P.H. are Research Associates of the FRS-FNRS. D.A. is a Research Fellow of the FRS-FNRS. S.L. and S.D.K. are Research Fellow and Postdoctoral Researcher of the FWO-Vlaanderen. L.W. was supported by EU project Tips4Cells. We thank K. Mc Evoy for helping us with data treatment.

REFERENCES AND NOTES

1. Beveridge, T. J.; Graham, L. L. Surface-Layers of Bacteria. *Microbiol. Rev.* **1991**, *55*, 684–705.
2. Costerton, J. W.; Stewart, P. S.; Greenberg, E. P. Bacterial Biofilms: A Common Cause of Persistent Infections. *Science* **1999**, *284*, 1318–1322.
3. Branda, S. S.; Vik, S.; Friedman, L.; Kolter, R. Biofilms: The Matrix Revisited. *Trends Microbiol.* **2005**, *13*, 20–26.

4. Ubbink, J.; Schar-Zammaretti, P. Probing Bacterial Interactions: Integrated Approaches Combining Atomic Force Microscopy, Electron Microscopy and Biophysical Techniques. *Micron* **2005**, *36*, 293–320.
5. Kolter, R.; Greenberg, E. P. Microbial Sciences: the Superficial Life of Microbes. *Nature* **2006**, *441*, 300–302.
6. Marco, M. L.; Pavan, S.; Kleerebezem, M. Towards Understanding Molecular Modes of Probiotic Action. *Curr. Opin. Biotechnol.* **2006**, *17*, 204–210.
7. Doron, S.; Snydman, D. R.; Gorbach, S. L. *Lactobacillus* GG: Bacteriology and Clinical Applications. *Gastroenterol. Clin. North Am.* **2005**, *34*, 483–498.
8. Tuomola, E. M.; Salminen, S. J. Adhesion of Some Probiotic and Dairy *Lactobacillus* Strains to Caco-2 Cell Cultures. *Int. J. Food Microbiol.* **1998**, *41*, 45–51.
9. Tuomola, E. M.; Ouwehand, A. C.; Salminen, S. J. The Effect of Probiotic Bacteria on the Adhesion of Pathogens to Human Intestinal Mucus. *FEMS Immunol. Med. Microbiol.* **1999**, *26*, 137–42.
10. Lebeer, S.; Verhoeven, T. L. A.; Perea Vélez, M.; Vanderleyden, J.; De Keersmaecker, S. C. J. Impact of Environmental and Genetic Factors on Biofilm Formation by the Probiotic Strain *Lactobacillus rhamnosus* GG. *Appl. Environ. Microbiol.* **2007**, *73*, 6768–6775.
11. Lebeer, S.; Claes, I. J. J.; Verhoeven, T. L. A.; Shen, C.; Lambrichts, I.; Ceuppens, J. L.; Vanderleyden, J.; De Keersmaecker, S. C. J. Impact of *luxS* and Supressor Mutations on the Gastrointestinal Transit of *Lactobacillus rhamnosus* GG. *Appl. Environ. Microbiol.* **2008**, *74*, 4711–4718.
12. Dufrêne, Y. F. Using Nanotechniques to Explore Microbial Surfaces. *Nat. Rev. Microbiol.* **2004**, *2*, 451–460.
13. Müller, D. J.; Dufrêne, Y. F. Atomic Force Microscopy as a Multifunctional Molecular Toolbox in Nanobiotechnology. *Nat. Nanotechnol.* **2008**, *3*, 261–269.
14. Schar-Zammaretti, P.; Ubbink, J. The Cell Wall of Lactic Acid Bacteria: Surface Constituents and Macromolecular Conformations. *Biophys. J.* **2003**, *85*, 4076–4092.
15. Touhami, A.; Jericho, M. H.; Beveridge, T. J. Atomic Force Microscopy of Cell Growth and Division in *Staphylococcus aureus*. *J. Bacteriol.* **2004**, *186*, 3286–3295.
16. Verbelen, C.; Dupres, V.; Menozzi, F. D.; Raze, D.; Baulard, A. R.; Hols, P.; Dufrêne, Y. F. Ethambutol-Induced Alterations in *Mycobacterium bovis* BCG Imaged by Atomic Force Microscopy. *FEMS Microbiol. Lett.* **2006**, *264*, 192–197.
17. Plomp, M.; Leighton, T. J.; Wheeler, K. E.; Hill, H. D.; Malkin, A. J. *In Vitro* High-Resolution Structural Dynamics of Single Germinating Bacterial Spores. *Proc. Natl. Acad. Sci. U.S.A.* **2007**, *104*, 9644–9649.
18. Dague, E.; Alsteens, D.; Latgé, J. P.; Dufrêne, Y. F. High-Resolution Cell Surface Dynamics of Germinating *Aspergillus fumigatus* Conidia. *Biophys. J.* **2008**, *94*, 656–660.
19. Touhami, A.; Nysten, B.; Dufrêne, Y. F. Nanoscale Mapping of the Elasticity of Microbial Cells by Atomic Force Microscopy. *Langmuir* **2003**, *19*, 4539–4543.
20. Pelling, A. E.; Sehati, S.; Gralla, E. B.; Valentine, J. S.; Gimzewski, J. K. Local Nanomechanical Motion of the Cell Wall of *Saccharomyces cerevisiae*. *Science* **2004**, *305*, 1147–1150.
21. Gaboriaud, F.; Bailet, S.; Dague, E.; Jorand, F. Surface Structure and Nanomechanical Properties of *Shewanella putrefaciens* Bacteria at two pH Values (4 and 10) Determined by Atomic Force Microscopy. *J. Bacteriol.* **2005**, *187*, 3864–3868.
22. Francius, G.; Tesson, B.; Dague, E.; Martin-Jezequel, V.; Dufrêne, Y. F. Nanostructure and Nanomechanics of Live *Phaeodactylum tricornutum* Morphotypes. *Environ. Microbiol.* **2008**, *10*, 1344–1356.
23. Dague, E.; Alsteens, D.; Latgé, J.-P.; Verbelen, C.; Raze, D.; Baulard, A. R.; Dufrêne, Y. F. Chemical Force Microscopy of Single Live Cells. *Nano Lett.* **2007**, *7*, 3026–3030.
24. Alsteens, D.; Dague, E.; Rouxhet, P. G.; Baulard, A. R.; Dufrêne, Y. F. Direct Measurement of Hydrophobic Forces on Cell Surfaces Using AFM. *Langmuir* **2007**, *23*, 11977–11979.
25. Dupres, V.; Menozzi, F. D.; Locht, C.; Clare, B. H.; Abbott, N. L.; Cuenot, S.; Bompard, C.; Raze, D.; Dufrêne, Y. F. Nanoscale Mapping and Functional Analysis of Individual Adhesins on Living Bacteria. *Nat. Methods* **2005**, *2*, 515–520.
26. Hinterdorfer, P.; Dufrêne, Y. F. Detection and Localization of Single Molecular Recognition Events Using Atomic Force Microscopy. *Nat. Methods* **2006**, *3*, 347–355.
27. Gilbert, Y.; Deghorain, M.; Wang, L.; Xu, B.; Pollheimer, P. D.; Gruber, H. J.; Errington, J.; Hallet, B.; Haulot, X.; Verbelen, C.; Hols, P.; Dufrêne, Y. F. Single-Molecule Force Spectroscopy and Imaging of the Vancomycin/D-Ala-D-Ala Interaction. *Nano Lett.* **2007**, *7*, 796–801.
28. Gad, M.; Itoh, A.; Ikai, A. Mapping Cell Wall Polysaccharides of Living Microbial Cells Using Atomic Force Microscopy. *Cell Biol. Int.* **1997**, *21*, 697–706.
29. Camesano, T. A.; Abu-Lail, N. I. Heterogeneity in Bacterial Surface Polysaccharides, Probed on a Single-Molecule Basis. *Biomacromolecules* **2002**, *3*, 661–667.
30. Camesano, T. A.; Liu, Y. T.; Datta, M. Measuring Bacterial Adhesion at Environmental Interfaces with Single-Cell and Single-Molecule Techniques. *Adv. Water Res.* **2007**, *30*, 1470–1491.
31. Abu-Lail, N. I.; Camesano, T. A. Polysaccharide Properties Probed with Atomic Force Microscopy. *J. Microsc.* **2003**, *212*, 217–238.
32. Lebeer, S.; De Keersmaecker, S. C. J.; Verhoeven, T. L. A.; Fadda, A. A.; Marchal, K.; Vanderleyden, J. Functional Analysis of *luxS* in the Probiotic Strain *Lactobacillus rhamnosus* GG Reveals a Central Metabolic Role Important for Growth and Biofilm Formation. *J. Bacteriol.* **2007**, *189*, 860–871.
33. Kasas, S.; Ikai, A. A Method for Anchoring Round Shaped Cells for Atomic-Force Microscope Imaging. *Biophys. J.* **1995**, *68*, 1678–1680.
34. Dufrêne, Y. F.; Boonaert, C. J. P.; Gerin, P. A.; Asther, M.; Rouxhet, P. G. Direct Probing of the Surface Ultrastructure and Molecular Interactions of Dormant and Germinating Spores of *Phanerochaete chrysosporium*. *J. Bacteriol.* **1999**, *181*, 5350–5354.
35. Boonaert, C. J. P.; Toniazzo, V.; Mustin, C.; Dufrêne, Y. F.; Rouxhet, P. G. Deformation of *Lactococcus lactis* Surface in Atomic Force Microscopy Study. *Colloids Surf., B* **2002**, *23*, 201–211.
36. Daniel, R. A.; Errington, J. Control of Cell Morphogenesis in Bacteria: Two Distinct Ways to Make a Rod-Shaped Cell. *Cell* **2003**, *113*, 767–776.
37. Formstone, A.; Carballido-Lopez, R.; Noirot, P.; Errington, J.; Scheffers, D. J. Localization and Interactions of Teichoic Acid Synthetic Enzymes in *Bacillus subtilis*. *J. Bacteriol.* **2008**, *190*, 1812–1821.
38. Burnham, N. A.; Colton, R. J. Measuring the Nanomechanical Properties and Surface Forces of Materials Using an Atomic Force Microscope. *J. Vac. Sci. Technol., A* **1989**, *A7*, 2906–2913.
39. Matzke, R.; Jacobson, K.; Radmacher, M. Direct, High-Resolution Measurement of Furrow Stiffening During Division of Adherent Cells. *Nat. Cell Biol.* **2001**, *3*, 607–610.
40. Rief, M.; Oesterhelt, F.; Heymann, B.; Gaub, H. E. Single Molecule Force Spectroscopy on Polysaccharides by Atomic Force Microscopy. *Science* **1997**, *275*, 1295–1297.
41. Marszalek, P. E.; Oberhauser, A. F.; Pang, Y. P.; Fernandez, J. M. Polysaccharide Elasticity Governed by Chair-Boat Transitions of the Glucopyranose Ring. *Nature* **1998**, *396*, 661–664.
42. Landersjo, C.; Yang, Z. N.; Huttunen, E.; Widmalm, G. Structural Studies of the Exopolysaccharide Produced by *Lactobacillus rhamnosus* Strain GG (ATCC 53103). *Biomacromolecules* **2002**, *3*, 880–884.

43. Francius, G.; Hemmerle, J.; Ball, V.; Lavalle, P.; Picart, C.; Voegel, J. C.; Schaaf, P.; Senger, B. Stiffening of Soft Polyelectrolyte Architectures by Multilayer Capping Evidenced by Viscoelastic Analysis of AFM Indentation Measurements. *J. Phys. Chem. C* **2007**, *111*, 8299–8306.
44. Riener, C. K.; Stroh, C. M.; Ebner, A.; Klampfl, C.; Gall, A. A.; Romanin, C.; Lyubchenko, Y. L.; Hinterdorfer, P.; Gruber, H. J. Simple Test System for Single Molecule Recognition Force Microscopy. *Anal. Chim. Acta* **2003**, *479*, 59–75.
45. Ebner, A.; Wildling, L.; Kamruzzahan, A. S. M.; Rankl, C.; Wruss, J.; Hahn, C. D.; Holzl, M.; Zhu, R.; Kienberger, F.; Blaas, D.; Hinterdorfer, P.; Gruber, H. J. A New, Simple Method for Linking of Antibodies to Atomic Force Microscopy Tips. *Bioconjug. Chem.* **2007**, *18*, 1176–1184.